Instrument Science Report COS 2010-01(v1)

SMOV Absolute Flux Calibration of the COS NUV Modes

Derck Massa[1], Alessandra Aloisi[1], Charles Keyes[1], Ralph Bohlin[1], and Cynthia Froning[2]
[1] Space Telescope Science Institute
[2]CASA, Univ. of Colorado

January 28, 2010

ABSTRACT

Initial point source sensitivity curves are determined for the COS NUV gratings: G230L, G185M, G225M and G285M. Observations through the PSA were obtained of the standard star GD71 at all central wavelength settings of all the gratings. In addition, PSA observations of the standard star GRW+70°5824 were obtained at selected settings. Because the pipeline used at the time of the analysis extracted BOA spectra incorrectly, BOA calibrations are not discussed here. The accuracy of the calibration is estimated to be ~ 2% for the medium resolution gratings, and somewhat less accurate for portions of the G230L. We also examine the contributions of off-order light contamination on the observed spectra. We find this to be negligible for the medium resolution gratings and for first order G230L spectra at wavelengths shorter than 3200Å.

Contents:

- Introduction (page 2)
- The Data (page 3)
- Derivation of the Response Curves (page 5)
- Overlapping orders in G230L Spectra (page 15)
- Second order contamination of first order spectra (page 15)
- First order contamination of second order spectra (page 17)

- Summary (page 17)
- Change History for COS ISR 2010-01 (page 18)
- References (page 18)

1. Introduction

One part of SMOV activities was to determine an initial absolute flux calibration for the COS NUV channel. The COS NUV channel consists of a grating and three separate camera mirrors which focus different portions of the spectrum onto a MAMA detector as three distinct stripes, termed Stripe A, B and C or segments NUVA, NUVB and NUVC. Thus, although we may refer to these three stripes as different segments, they are, in fact, simply different regions of the same detector. In addition, for the low resolution grating, G230L, the light falling on Stripe C is expected to be predominantly from the grating's second order. For the medium resolution gratings, G185M, G225M and G285M, the light in all of the stripes is expected to be dominated by the first order spectrum (see, the *COS Instrument Handbook*, Dixon et al. 2010 for more details).

In principle, absolute flux calibration is a straightforward procedure which can be accomplished in the following steps:

- Obtain observations of one or more standard stars for each instrumental configuration.
- Process the data to the point where it can be cast into the form of a linearized counts spectrum, $C(x)$ (counts s^{-1}pixel^{-1}).
- Ratio the counts spectra with the calibrated flux spectra $F(\lambda)$ (ergs cm^{-2}s^{-1}Å^{-1}) of standard stars. This produces the observed (or raw) point source sensitivity curve, defined as
$$S(\lambda) = C(x)/F(\lambda), \quad (1)$$
- Produce a smooth version of the observed sensitivity curve which, when multiplied by the counts spectrum, transforms counts s^{-1}pixel^{-1} to ergs cm^{-2}s^{-1}Å^{-1}. For COS data, the input would be the `net` spectrum contained in the first extension of the `x1d` files.

Traditionally, the absolute flux calibration is envisioned as a smooth function which summarizes the wavelength dependence of the optical properties of the gratings and mirrors. It is normally assumed that the detector properties (which can vary rapidly with wavelength) have been removed through the process of "flat fielding" the detector. For the COS MAMA, this is an excellent approximation. However, at the time the calibration described in this ISR was done, the COS MAMA flat field and bad pixel maps had not been updated from their pre-flight values. As a result, the data used in

the calibration described here are somewhat noisier than data currently being processed through calcos using the updated files. Nevertheless, this does not have a significant effect on the flux calibration, which assumes a smooth response curve.

A further limitation of the calibration described in this ISR is that it does not include a calibration of BOA spectra. This is because the calibration files used by calcos at the time of the calibration did not properly extract the BOA data. This situation has subsequently been corrected.

In the following sections, we describe the data used in the analysis (§2), derive the sensitivity curves (§ 3), discuss the effects of overlaping orders on the G230L data (§ 4), and summarize our results (§ 5).

2. The Data

The data used in the calibration, were all of the available standard star observations from program 11479 available on 8/14/09. This program was designed to obtain observations of standard stars at all of the central wavelength positions of all of the gratings of the COS NUV channel. The files used in the analysis are listed in Table 1. The data were processed by `OPUS` version 2009_2g and `calcos` version 2.10. The calibration files used by `calcos` included PSA extraction windows determined from in flight data and a flat field calibration file composed of the pre-launch flat field measurements adjusted to include the "RAMP correction", which simulates the effects of vignetting (see, ISR Ake et al. 2020).

Data for both GRW+70°5824 and GD71 were used. The intrinsic SEDs used to create the sensitivity curves from these data were Bohlin's best fit model for GD71 (Bohlin 2003), and his STIS spectrum for GRW+70°5824. Both of these data sets are available at the CALSPEC website
`http://www.stsci.edu/hst/observatory/cdbs/calspec.html`
Specifically, the standard star files used were `grw_70d5824_stisnic_002.fits` and `gd71_mod_006.fits`.

Table 1. Files used in the analysis.

File	Target	Grating	λ_c
laad01klq_x1d.fits	GRW+70D5824	G185M	1786
laad02e8q_x1d.fits	GD71	G185M	1786
laad02eaq_x1d.fits	GD71	G185M	1786
laad02edq_x1d.fits	GD71	G185M	1817
laad02efq_x1d.fits	GD71	G185M	1835
laad01knq_x1d.fits	GRW+70D5824	G185M	1850
laad02ehq_x1d.fits	GD71	G185M	1850
laad02ejq_x1d.fits	GD71	G185M	1864
laad02elq_x1d.fits	GD71	G185M	1882
laad02enq_x1d.fits	GD71	G185M	1890
laad02epq_x1d.fits	GD71	G185M	1900
laad02erq_x1d.fits	GD71	G185M	1913
laad02etq_x1d.fits	GD71	G185M	1921
laad02evq_x1d.fits	GD71	G185M	1941
laad02exq_x1d.fits	GD71	G185M	1953
laad02ezq_x1d.fits	GD71	G185M	1971
laad02f1q_x1d.fits	GD71	G185M	1986
laad02f3q_x1d.fits	GD71	G185M	2010
laad02f5q_x1d.fits	GD71	G185M	2010
laad01kfq_x1d.fits	GRW+70D5824	G225M	2186
laad02dcq_x1d.fits	GD71	G225M	2186
laad02deq_x1d.fits	GD71	G225M	2186
laad02dgq_x1d.fits	GD71	G225M	2217
laad02diq_x1d.fits	GD71	G225M	2233
laad01kbq_x1d.fits	GRW+70D5824	G225M	2250
laad02d9q_x1d.fits	GD71	G225M	2250
laad02dkq_x1d.fits	GD71	G225M	2268
laad02dmq_x1d.fits	GD71	G225M	2283
laad02doq_x1d.fits	GD71	G225M	2306
laad02dqq_x1d.fits	GD71	G225M	2325
laad02dsq_x1d.fits	GD71	G225M	2339
laad02duq_x1d.fits	GD71	G225M	2357
laad02dwq_x1d.fits	GD71	G225M	2373
laad02dyq_x1d.fits	GD71	G225M	2390
laad02e0q_x1d.fits	GD71	G225M	2410
laad02e6q_x1d.fits	GD71	G225M	2410
laad01kjq_x1d.fits	GRW+70D5824	G230L	2635
laad02fdq_x1d.fits	GD71	G230L	2635
laad02ffq_x1d.fits	GD71	G230L	2635
laad02frq_x1d.fits	GD71	G230L	2950
laad02fwq_x1d.fits	GD71	G230L	3000
laad01khq_x1d.fits	GRW+70D5824	G230L	3000
laad02fhq_x1d.fits	GD71	G230L	3360

Table 1. (cont'd)

File	Target	Grating	λ_c
laad02foq_x1d.fits	GD71	G230L	3360
laad01kpq_x1d.fits	GRW+70D5824	G285M	2617
laad03vxq_x1d.fits	GD71	G285M	2617
laad03vzq_x1d.fits	GD71	G285M	2617
laad03w4q_x1d.fits	GD71	G285M	2637
laad01krq_x1d.fits	GRW+70D5824	G285M	2850
laad03w7q_x1d.fits	GD71	G285M	2657
laad03y7q_x1d.fits	GD71	G285M	2676
laad03wbq_x1d.fits	GD71	G285M	2695
laad03wdq_x1d.fits	GD71	G285M	2709
laad03wfq_x1d.fits	GD71	G285M	2719
laad03wmq_x1d.fits	GD71	G285M	2739
laad03woq_x1d.fits	GD71	G285M	2850
laad03wqq_x1d.fits	GD71	G285M	2952
laad03wyq_x1d.fits	GD71	G285M	2979
laad03xuq_x1d.fits	GD71	G285M	2996
laad03xyq_x1d.fits	GD71	G285M	3018
laad03y0q_x1d.fits	GD71	G285M	3035
laad03y3q_x1d.fits	GD71	G285M	3057
laad03y5q_x1d.fits	GD71	G285M	3074
laad01kvq_x1d.fits	GRW+70D5824	G285M	3094
laad02f7q_x1d.fits	GD71	G285M	3094
laad03w9q_x1d.fits	GD71	G285M	3094

3. Derivation of the Sensitivity Curves

To construct the sensitivity curves, we began with the `net` spectra from the `x1d` files. All of the central wavelength positions for a single grating and stripe were analyzed together. The net spectra for each observation of each standard were divided by the corresponding CALSPEC standard star flux (interpolated onto the observed wavelength grid) to produce raw sensitivity curves. The raw curves (trimmed to eliminate the first and last 115 points which can be either devoid of data or else populated by drift corrections due to grating motions) were then concatenated into a single, large array of all the raw sensitivity curves and sorted by wavelength (sensitivity curves derived from GD71 and GRW+70°5824 data are identical within the noise). The concatenated raw curves, binned by 10 points, are compared to the pre-launch expectations in Figures 1–5.

Several points can be seen from an examination of the raw sensitivity curves.

- The individual stripes have distinctly different responses, with Stripe A always being more sensitive than Stripe B in the region of overlap, and Stripe B always being more sensitive than Stripe C in their overlapping regions. This arises because each stripe has its own focusing mirror, so it appears that the mirror for A

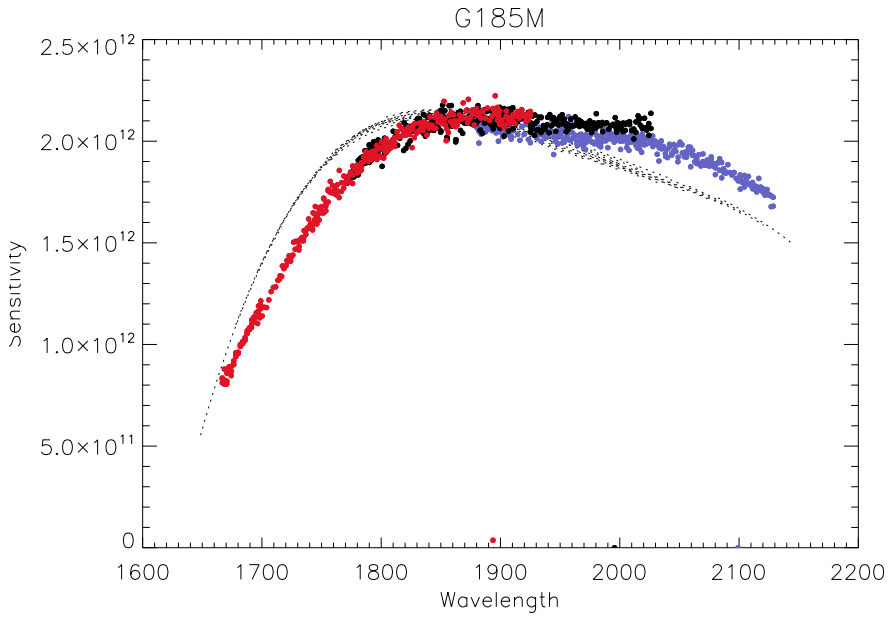

Figure 1. Empirical sensitivity curves for the three stripes of the G185M grating, using all of the available data. Red = NUVA, black = NUVB, blue = NUVC. Dashed curves are the pre-launch estimates.

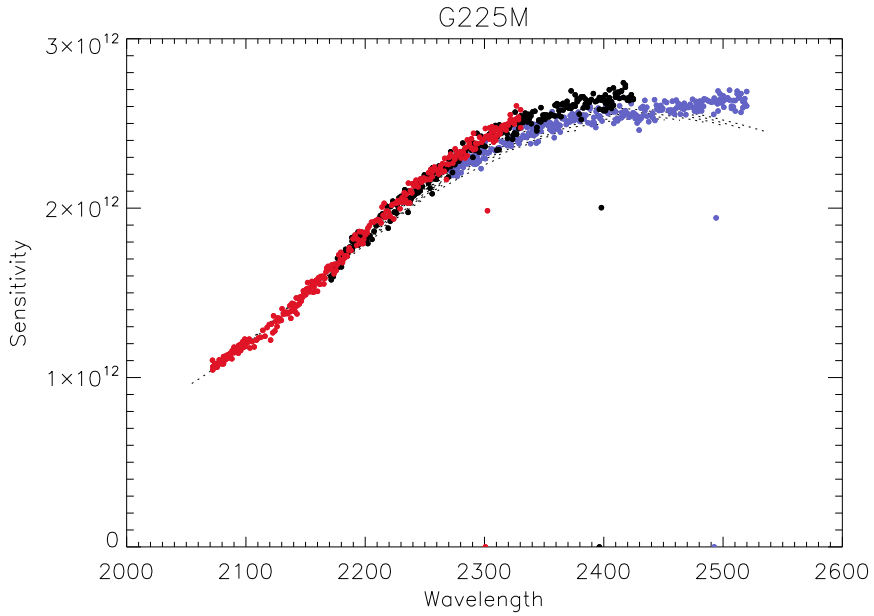

Figure 2. Same as Figure 1 for G225M.

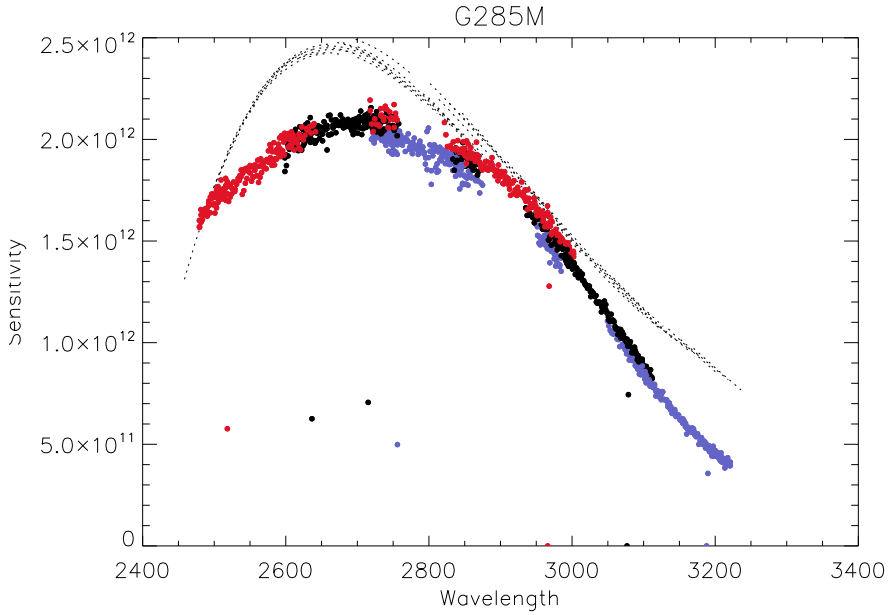

Figure 3. Same as Figure 1 for G285M.

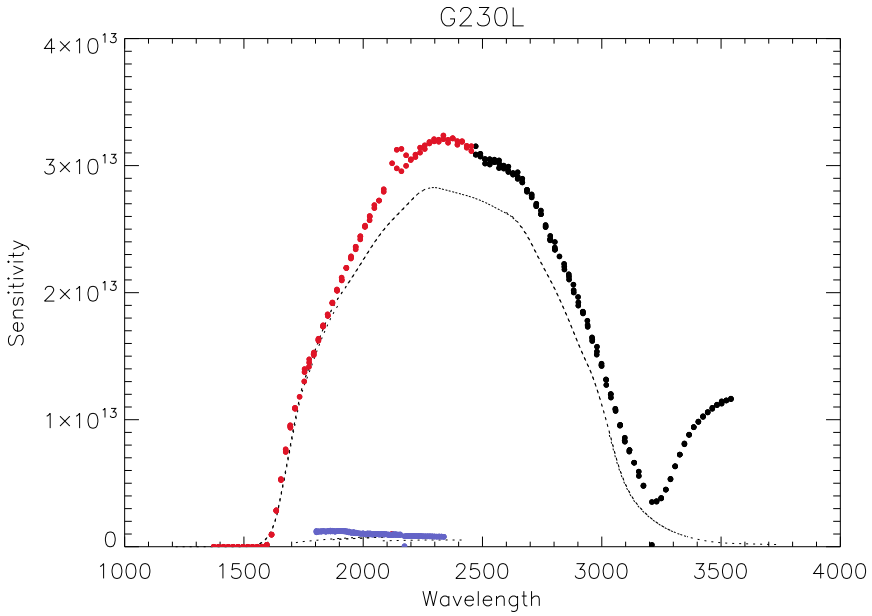

Figure 4. Same as Figure 1 for G230L.

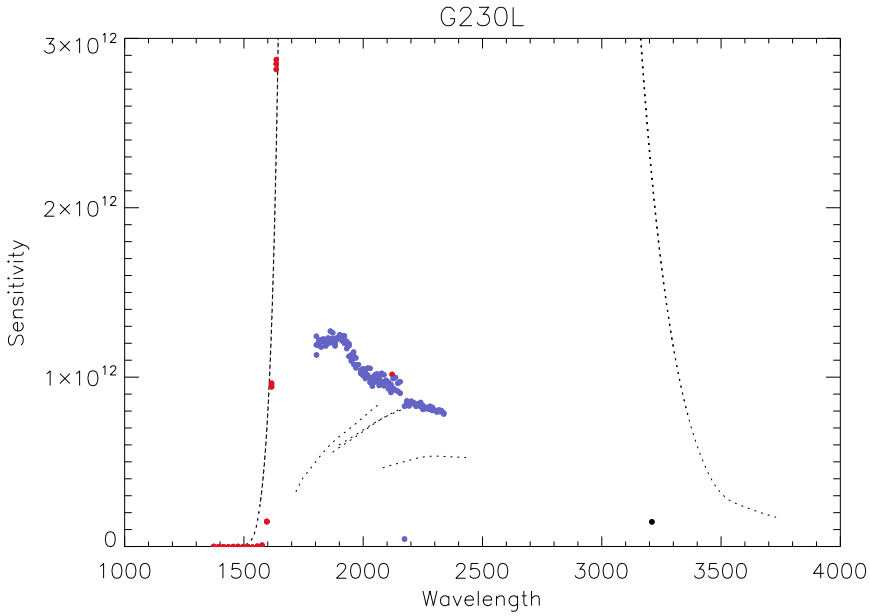

Figure 5. Same as Figure 1 for G230L, emphasizing the second order responses.

is more efficient than the one for B and that the one for B is more efficient than the one for C.

- Unlike the other gratings, data from a single G285M stripe cannot cover the full wavelength range of that stripe, even when all of the available central wavelength settings are combined. However, the entire wavelength range of the grating is covered by combinations of all the central wavelengths and stripes.

- The response for the G285M deviates strongly from its pre-launch measurements. This was expected, since both the G225M and G285M gratings are bare aluminium, and were expected to degrade between testing and launch since they can react with air. However, it appears that only the G285M was affected. We will continue to monitor these gratings for further changes.

- The long wavelength portion of the curve for G230L, NUVB, CENWAVE = 3360Å, deviates strongly from pre-launch expectations, as do all G230L NUVC (second order) curves. The reasons for these discrepancies are addressed in § 4.

- There are a few "wild points" in the curves. These arise from two sources. One is interstellar lines in GD71 that are not included in the model we used for its intrinsic flux. The second is that we ignored the bad pixel maps during this initial calibration.

- The apparent reduction in the scatter at longer wavelengths in Figures 16 and 17

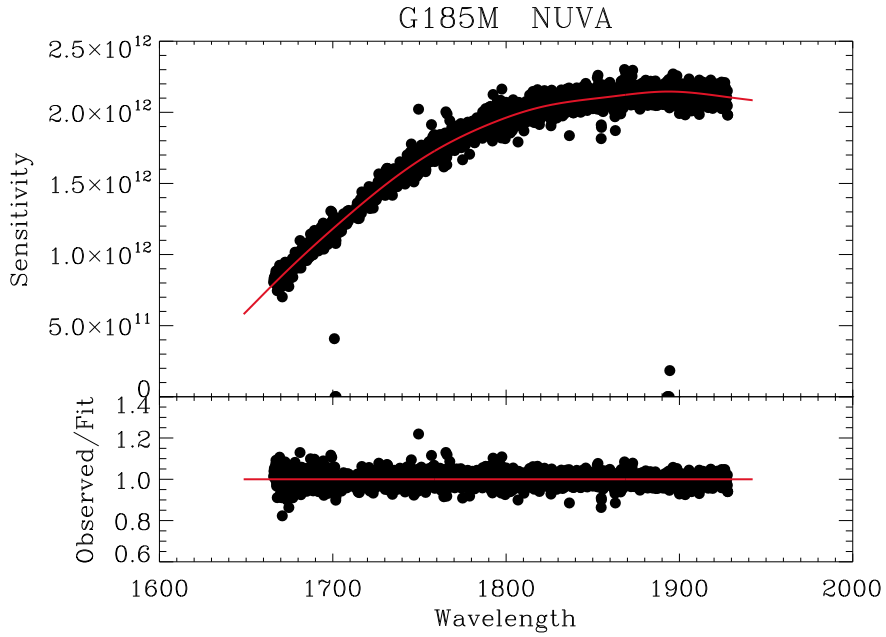

Figure 6. Fit to the G185M-NUVA for all central wavelengths. The upper panel shows the binned data and the fit (in red), and the lower panel shows the ratio of the observed data by the fit, compared to unity (the red line).

results because only the brighter standard, GD71, was observed at those wavelengths.

The sensitivity curves for each grating and stripe were fit individually. In each case, the data for both standards were combined. A fit to these curves was determined using a spline through a set of selected points. The exact location of the points is subjective at present, but will become standardized over the next few iterations of the curves, once the new flat field and bad pixel map are in place.

The resulting fits for each grating and stripe combination are shown in Figures 6–17. Each figure shows the fit to the raw sensitivity curve in the top panel. The lower panel shows the ratio of the raw data divided by the fit. In most cases there is very little evidence for residual low frequency deviations, and the fits are consistent with an accuracy of $\sim$ 2%. However, there are a few problem areas that will have to be addressed in future calibrations. These are confined to the G230L and are related to the following:

1. Rapid changes in the curvature at the short wavelength end of NUVA and the long wavelength end of NUVB. Additional spline points should handle the short wavelength end of the NUVA, and the long wavelength end of the NUVB will be eliminated in later calibrations since it is strongly contaminated by second order light (see § 4).

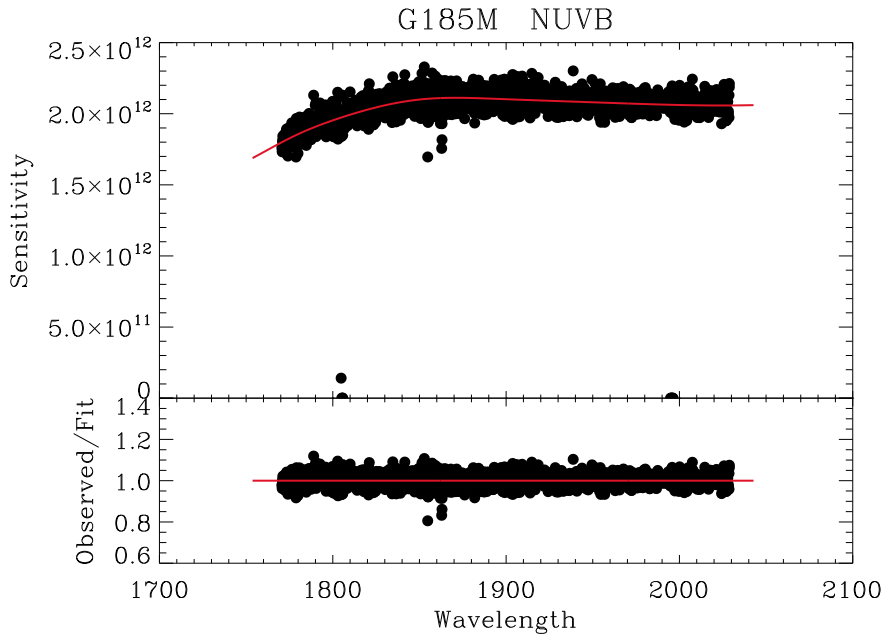

Figure 7. Same as Figure 6 for G185M-NUVB.

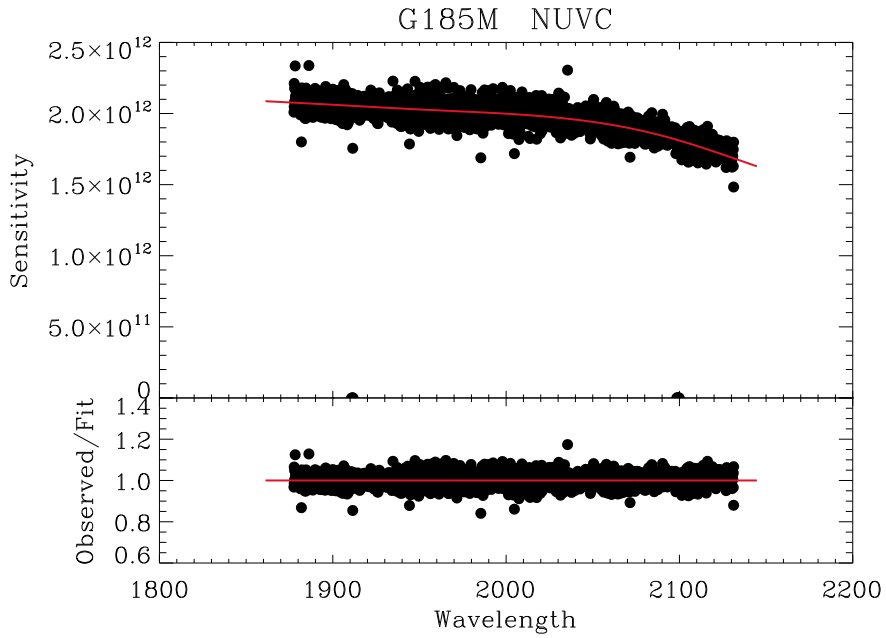

Figure 8. Same as Figure 6 for G185M-NUVC.

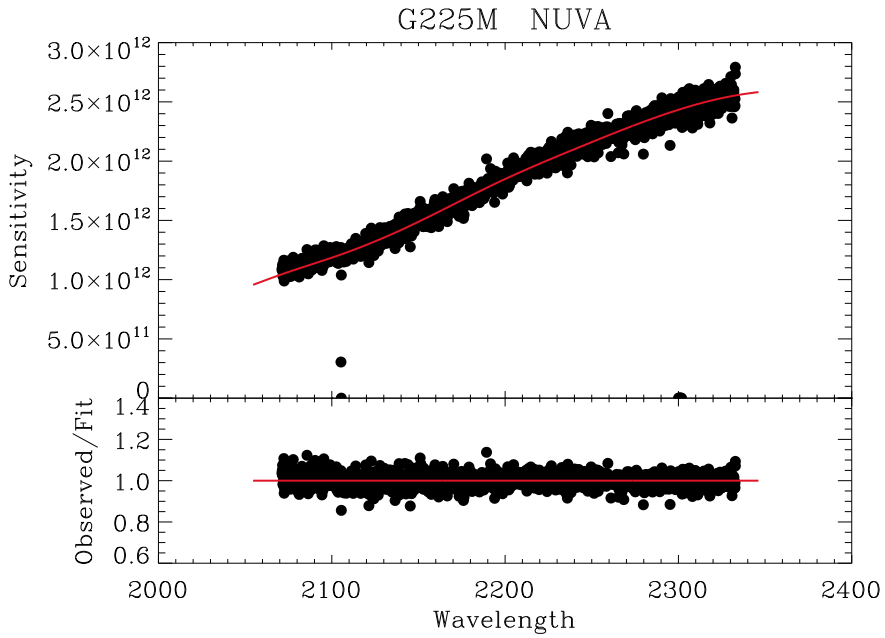

Figure 9. Same as Figure 6 for G225M-NUVA.

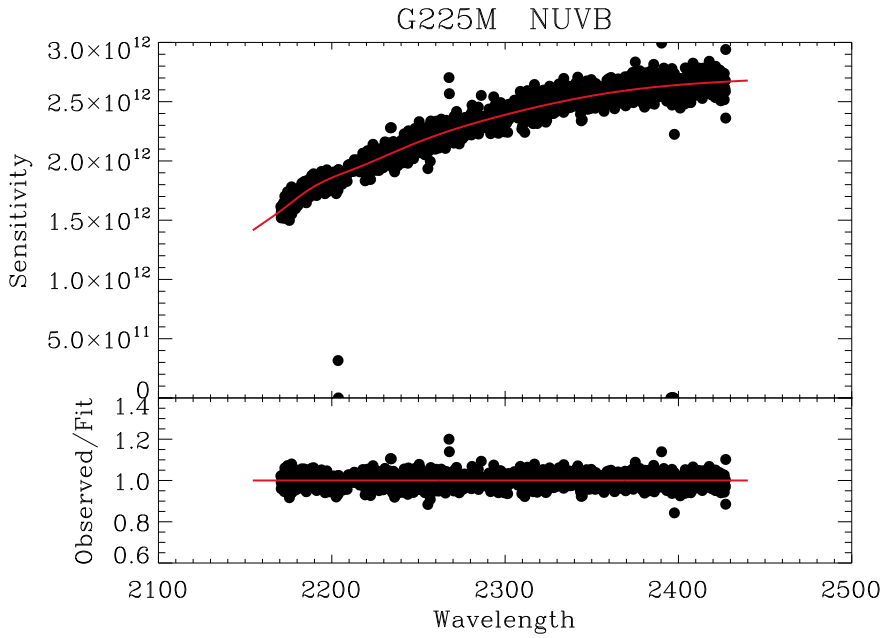

Figure 10. Same as Figure 6 for G225M-NUVB.

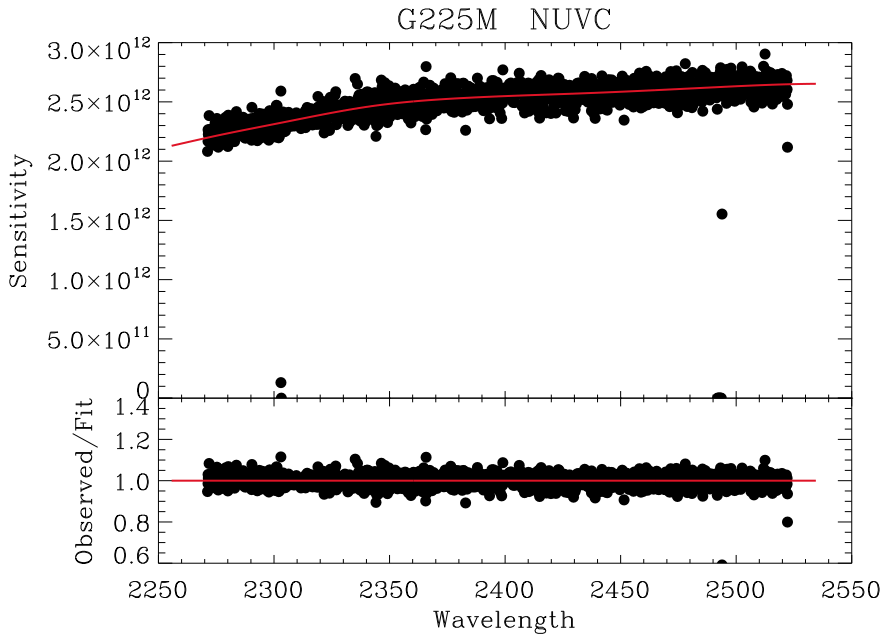

Figure 11. Same as Figure 6 for G225M-NUVC.

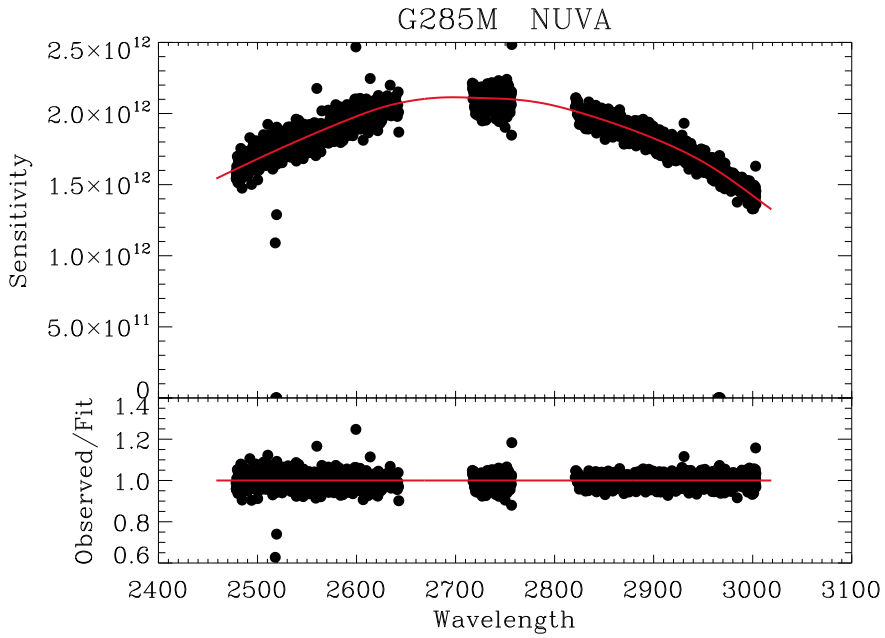

Figure 12. Same as Figure 6for G285M-NUVA.

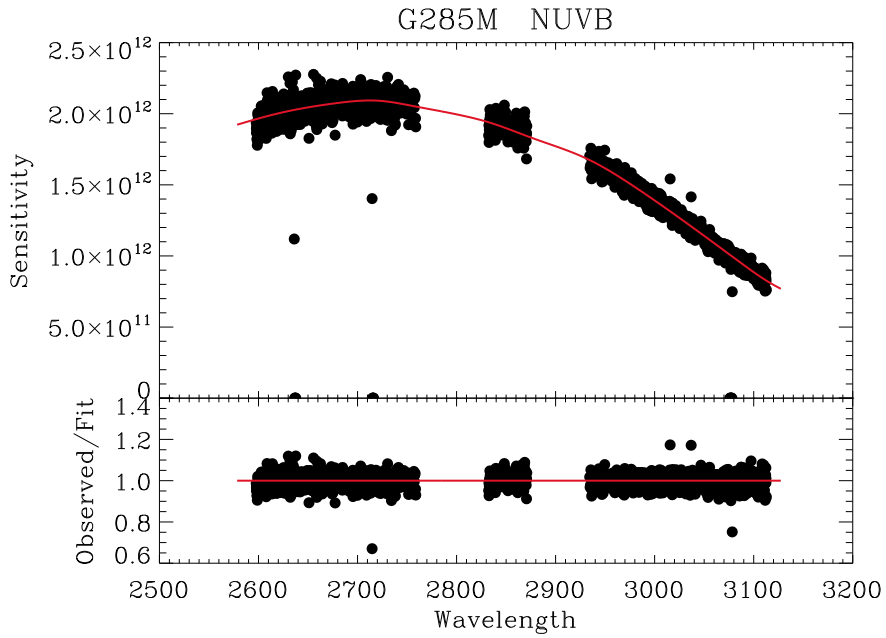

Figure 13. Same as Figure 6 for G285M-NUVB.

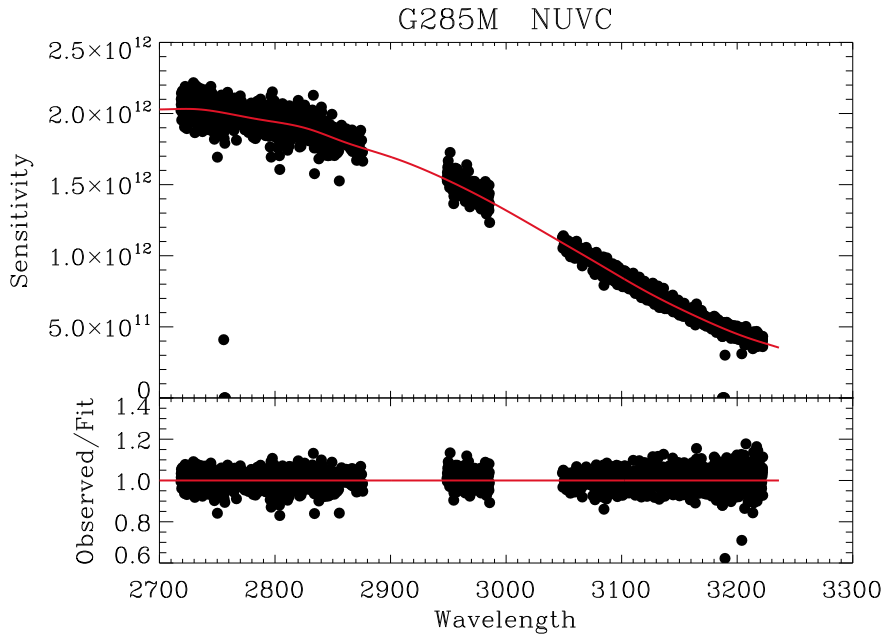

Figure 14. Same as Figure 6 for G285M-NUVC.

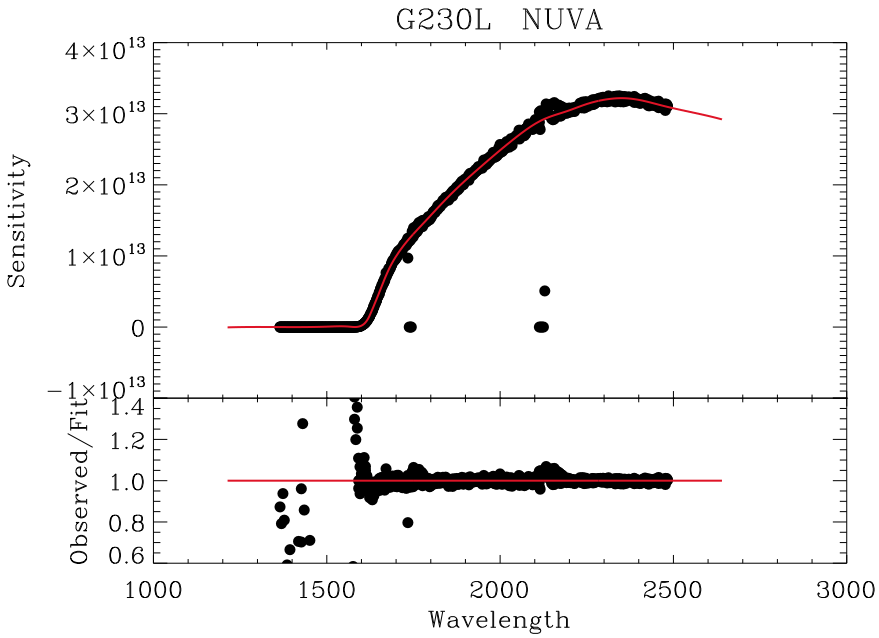

Figure 15. Same as Figure 6 for G230L-NUVA.

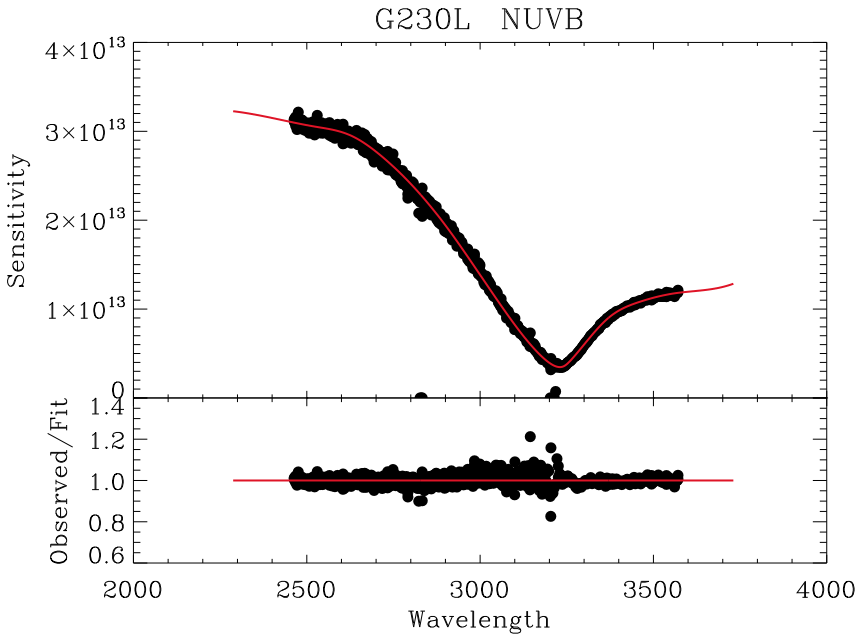

Figure 16. Same as Figure 6 for G230L-NUVCB.

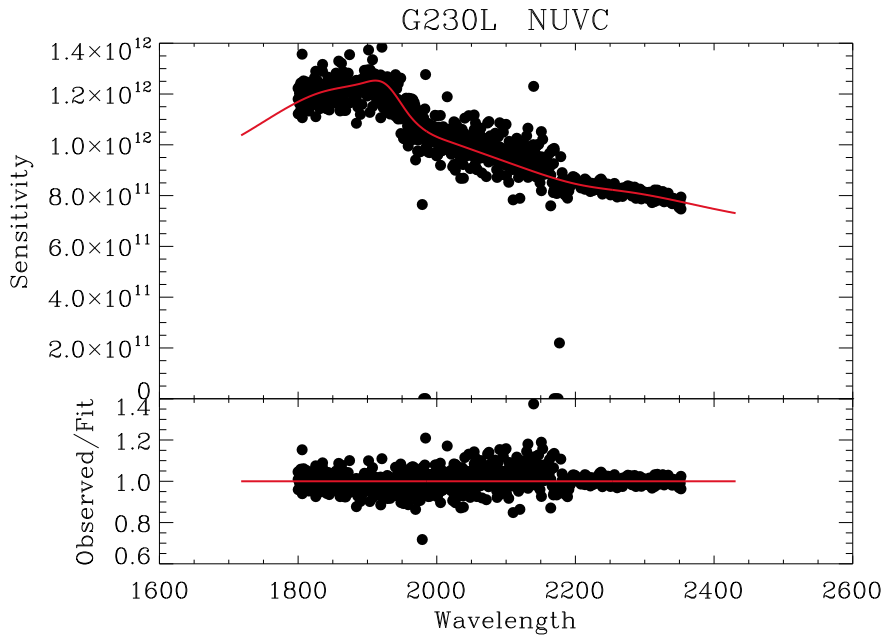

Figure 17. Same as Figure 6 for G230L-NUVC.

2. The NUVC spectra are problematic, and it is not certain how useful these spectra will be. This is because they are also combinations of overlapping orders (see § 4).

4. Overlapping Orders in G230L Spectra

In performing the NUV flux calibration, it was apparent that the second order contribution to the longer wavelengths of the G230L spectra was substantial. It was also noticed that the apparent response of the second order stripe (NUVC) of the G230L was very different than expected. Both of these effects turn out to be related to overlapping spectral orders. In this section, we compare the distinctive emission lines in COS NUV spectra of the Planetary Nebula NGC 6833 to existing FOS spectra obtained through its $1''$ aperture. Both sets of observations should include the bulk of the nebular emission.

The COS data are from program 11474 (obtained through 18 Aug. 2009). The archival FOS spectra for NGC 6833 (all obtained through the $1''$ aperture) are Y2DE010FT for the G190M grating (for $1600 \leq \lambda \leq 2300$) and Y2DE020CT for the G400H grating ($3200 \leq \lambda \leq 4800$).

4.1 Second order contamination of first order spectra

The apparent upturn in the G230L NUVB sensitivity long ward of 3200Å is actually the result of the overlapping second order light at half the wavelength, i.e., $\lambda \geq 1600$Å. To obtain a rough estimate of the contributions of the two orders to the COS spectrum, we

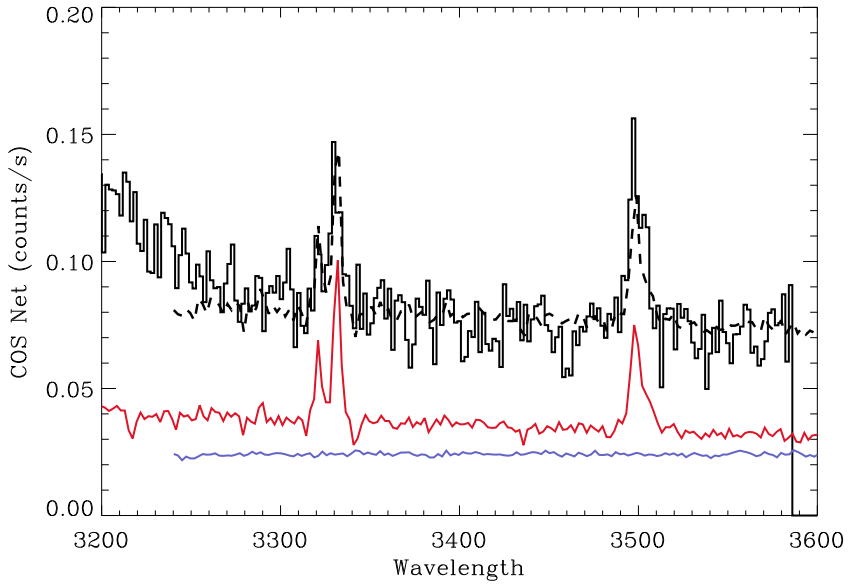

Figure 18. The black curve is the G230L NUVB CENWAVE = 3360 spectrum of NGC 6833; the blue curve is an FOS spectrum over the same wavelength range, and; the red curve is an FOS spectrum of the region $1600 \leq \lambda \leq 1800$Å, plotted as $f(2\lambda)$. The FOS spectra have been rescaled by arbitrary amounts for display purposes. The dashed curve is a combination of the two FOS spectra which provides a good representation of the COS spectrum. The ratio of the scale factors used to obtain this fit is a measure of the ratio of the first and second order light contributions to the COS spectrum.

simply rescaled the flux calibrated FOS data and then plotted sums of the FOS spectrum at the COS wavelengths and at half of the COS wavelengths. These represent the first and second order contributions. The ratio of the scale factors needed to make the two FOS spectra reproduce the COS spectrum, gives the ratio of the first and second order light contributions.

Figure 18 shows the G230L NUVB CENWAVE = 3360 COS data as a black spectrum, which has two strong emission lines. The blue spectrum is the FOS spectrum over the same region. Unlike the COS spectrum, it is featureless. On the other hand, the red spectrum, which is the FOS spectrum for $1600 \leq \lambda \leq 1800$Å, plotted as $f(2\lambda)$, contains strong emission lines at the same "wavelengths" where they appear in the COS spectrum. Thus, it is obvious that the emission lines originate from the overlapping second order spectrum. The dashed curve is a sum of the two flux calibrated FOS spectra, rescaled to match the COS spectrum near 3300Å. To sum consists of 40% of the second order flux (the red spectrum) and 60% of the first order flux (the blue spectrum). The fact that it agrees well with the emission lines near 3320Å indicates that $\sim 40\%$ of the COS spectrum is second order light at that wavelength. Similarly, the fact that this ratio underestimates the emission line near 3500Å, indicates that the COS spectrum

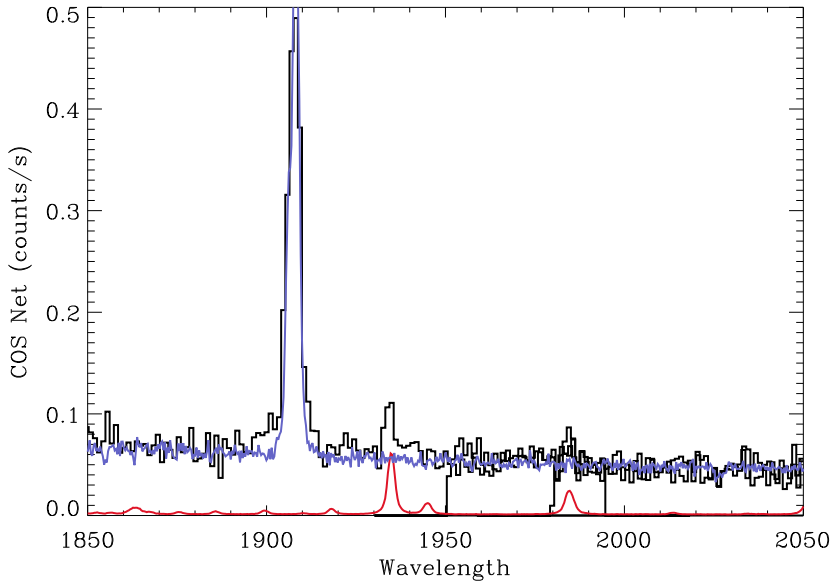

Figure 19. The Black curve is all of the G230L NUVC spectra for NGC 6833; the blue curve is an FOS spectrum for the same wavelength interval, and the red curve is an FOS spectrum of the region $3700 \leq \lambda \leq 4100$Å, plotted as $f(\lambda/2)$. The FOS spectra have been rescaled by arbitrary amounts for display purposes.

contains an even larger second order contribution at that wavelength.

Finally, we note that Figure 15 shows that the response of the NUV spectrograph is effectively zero for $\lambda \leq 1600$Å. This implies that second order contamination should be negligible for all of the medium resolution gratings, and for G230L NUVB data shortward of 3200Å.

4.2 First order contamination of second order spectra

Figure 19 shows the G230L Stripe C second order COS spectrum (in black) along with FOS spectra covering the same wavelength range (blue spectrum) and from twice the observed wavelengths (red). The latter represents the contribution of an overlapping first order spectrum. It has been scaled to 5% of the blue spectrum, so that it shows how a 5% contribution from first order would affect the resulting spectrum. Given the S/N of the available data, 5% appears to be a reasonable estimate for the first order contribution. We do not combine the FOS spectra in this case, since the first order spectrum has very little continuum and its contribution to the COS spectrum is obvious.

5. Summary

The major results of this ISR are the following:

1. The current NUV calibration for the medium resolution gratings should be accurate to $\sim 2\%$.

2. The accuracy for portions of the G230L data may be somewhat less, due to rapid changes in the curvature of the sensitivity as a function of wavelength, which makes it difficult to characterize.

3. G230L data for wavelengths ≥ 3200Å can be strongly contaminated by second order light.

4. G230L NUVC spectra are predominantly second order, but they can contain a contribution from longer, first order light.

5. All of the medium resolution grating data and the first order G230L data shortward 3200Å should be free of second order contributions.

6. Change History for COS ISR 2010-01

Version 1: 28 January 2010 - Original Document.

References

Ake, T. B., Burgh, E. B., Penton, S. V. 2010, COS Instrument Science Report 2010-03

Bohlin, R. 2003, 2002 HST Calibration Workshop, ed. S. Arribas, A. Koekemoer, & B. Whitmore, (Baltimore:STScI), p. 115

Dixon, W. V., et al. 2010, "Cosmic Origins Spectrograph Instrument Handbook", Version 2.0 (Baltimore:STScI)